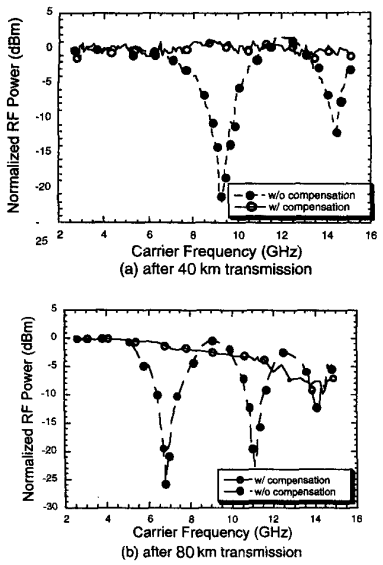

CWK2 Fig. 2. RF power versus subcarrier frequencies w/ and w/o compensation for (a) 40-km and (b) 80-km transmission.

Figure 1(b) shows the wavelength-dependent time delay under different stretching voltages. The slope of the curve (i.e., the dispersion) at the operating laser wavelength can be changed by varying the PZT voltage. This grating enables compensation of dispersion accumulated for various distances as well as the dispersion accumulated in *multiple* subcarriers.

Figures 2(a) and 2(b) show the effect of compensation for RF power degradation after 40 and 80 km transmission, respectively. Compensation can be achieved for a continuous carrier frequency range of 2–14 GHz, but our technique can generically accommodate much higher frequencies.

Figure 3(a) shows the received RF power as a function of applied PZT voltage. The received RF power can be tunably compensated by changing the voltage, and <0.5-dB power fading can be achieved. Figure 3(b) shows the RF spectrum of a 6.3-GHz subcarrier with and without compensation after 40 and 80 km transmission. The power degradations can be compensated by tuning the FBG, thereby providing optical network flexibility and robustness. After 40- and 80-km transmission, a 5.5- and 14.8-dB degradation, respectively, is generated and compensated by tuning the grating. Another significant advantage of our all-optical technique is that multiple subcarrier channels can be compensated simultaneously by a single grating. In Fig. 3(c), the two SCM channels experience different RF degradation since they have different subcarrier frequencies. The 6.3-GHz subcarrier experiences a 14.3-dB fading and the 7.5-GHz subcarrier experiences a 6.9-dB degradation. The RF power of the two channels can be almost completely compensated simultaneously by tuning the grating. Note that the degradation of more than two SCM channels can also be compensated by our grating.

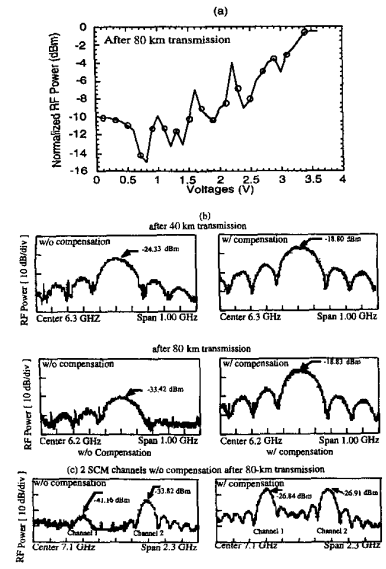

CWK2 Fig. 3. (a) RF power versus tuning voltages on the nonlinearly-chirped FBG. (b) RF spectum w/ and w/o tunable dispersion compensation after 40/80 km of fiber. (c) RF spectrum of two subcarrier channels w/ and w/o tunable dispersion compensation.

1. J. Marti, D. Pastor, M. Tortola, and J. Capmany, Electron. Lett., vol. **32,** no. 3, pp 236–237, 1996.
2. G.H. Smith, D. Novak, *et al.*, Electron. Lett. 33, 1159–1160, 1997.
3. C. Lim, D. Novak, *et al.*, in OFC '98, Paper TuC3.
4. J. Marti, J.M. Fuster and R.I. Laming, Electronics Lett, vol. **33,** no. 13, pp 1170–1171, 1997.
5. K.-M Feng, V. Grubsky, D. Starodubov, J.-X. Cai, A.E. Willner, and J. Feinberg, in OFC '98, Paper TuM3.

CWK3 **3:45 pm**

Noise suppression properties of distributed balanced photodetectors for high performance RF photonic links

M. Saiful Islam, Tai Chau, Sagi Mathai, Tatsuo Itoh, Ming C. Wu, *UCLA Electrical Engineering Department, 63-128 Engineering IV, 405 Hilgard Avenue, Los Angeles, California 90095-1594 USA; E-mail: wu@ee.ucla.edu*

Balanced photodetectors are of great interest to analog fiber optic links because they can suppress relative intensity noise (RIN) of lasers and amplified spontaneous emission noise (ASE) from erbium-doped fiber amplifiers (EDFA). When used in conjunction with an external modulator with complementary outputs, shot noise-limited system performance can be achieved.[1] In order to fully exploit the advantages of the balanced systems, balanced photodetectors with high saturation photocurrents and broad bandwidth are required. Monolithically integrated balanced photodetectors offer superior performance (broader bandwidth, better matching of photodiodes) and reduced packaging cost. However, most of the integrated balanced photodetectors reported to date have low saturation photocurrents and are not suitable for analog applications.

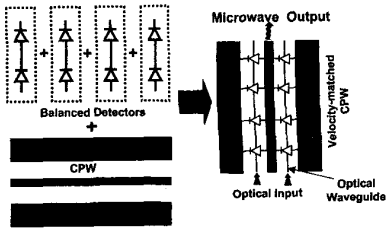

CWK3 Fig. 1. Principle and schematic structure of the distributed balanced photodetector. We cascaded multiple balanced photodetector pairs in series along a coplanar waveguide to increase saturation photocurrent.

Previously, we have reported a novel distributed balanced photodetector.[2] It integrates two velocity matched distributed photodetectors (VMDP) with a microwave coplanar waveguide (CPW). This new device inherits the basic advantages of the VMDP, namely, broad bandwidth and high saturation photocurrent.[3] In this paper, we reported on the noise suppression properties of the monolithic balanced distributed photodetector. A high signal-to-noise (SNR) and large suppression of the laser RIN over a broad range of input powers has been observed in the RF photonic link employing the balanced VMDP.

Figure 1 shows the schematic of the balanced distributed photodetector. It consists of two input optical waveguides, two arrays of high-speed metal-semiconductor-metal (MSM) photodiodes distributed along the optical waveguides, and a 50Ω coplanar waveguide (CPW) output transmission line. By biasing the photodiodes in balanced mode, only the *difference photocurrents* are collected by the CPW. The balanced VMDP showed a RIN suppression of more than 17 dB with a very good common mode rejection ratio (CMRR) >27 dB.

An RF photonic link with a dual-output complementary Mach-Zehnder modulator (MZM) has been set up to characterize the noise properties of the distributed balanced receiver. The RF carrier is fixed at 6.5 GHz. Figure 2 shows the SNR of the link versus the received optical power for both the distributed balanced receiver and the reference receiver with a single detector. The SNR for the single detector receiver is almost constant with increasing optical power, indicating that the receiver noise is dominated by the RIN. In contrast, the SNR for the balanced receiver increases monotonically with optical power upto 15 mW. For optical power greater than 15 mW, the SNR still increases monotonically with optical power at a smaller rate. This suggests the presence of some residue RIN. Comparing the two receivers, it is also noted that the SNR for balanced receiver is 23 dB higher than the single detector receiver.

The RF signals detected by the balanced detector should be exactly at 180° out of phase for optimum noise suppression. This requires the lengths of the fiber from the complimen-

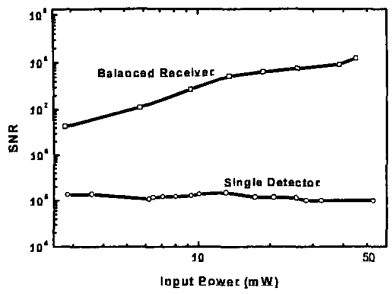

CWK3 **Fig. 2.** Measured signal-to-noise ratio (SNR) of the balanced receiver. The lower curve shows the SNR for the receiver in unbalanced configuration.

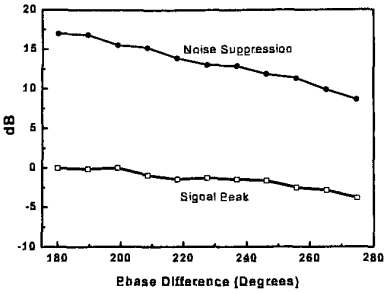

CWK3 **Fig. 3.** Total amount of noise suppression and the deviation of the signal peak versus phase deviation of the RF signal from 180°. Even with a phase variation of 100°, the receiver can suppress more than 9 dB of RIN noise whereas the signal peak reduction was less than 4 dB.

tary MZM to the detector to be exactly the same in length. In practical applications, the optical path length will drift slightly due to environmental changes and it is important to understand the impact of phase mismatch. Figure 3 plots the variation in the signal peak and the amount of noise suppression when the phase difference at the RF signal at 6.5 GHz deviates from 180°. The measured data shows that even with a phase variation of 100°, our device can suppress more than 9 dB of RIN noise whereas the signal peak reduction was less than 4 dB. As balanced detector amplifies the RF signal by 6 dB, with a phase deviation of 100°, the signal is still higher than that of an unbalanced detector. For the RF signal of 6.5 GHz, 100° phase variation between two fibers corresponds to ~8.5 mm of fiber length.

In conclusion, we measured the SNR and phase tolerance of the input RF signals of the high power distributed balanced receiver. This monolithic balanced receiver has the potential to dramatically improve the performance of RF photonic links.

This project is supported in part by ONR MURI on RF Photonics, National Radio Astronomy Observatory, JESP and UC MICRO.

1. L.T. Nichols, K.J. Williams, R.D. Esman, "Optimizing the Ultrawide-band photonic link," *IEEE Trans. Microwave Theory and Techniques*, vol. **45**, no. 8, pp. 1384–1389, 1997.
2. M.S. Islam, T. Chau, S. Mathai, A. Rollinger, A. Nespola, W.R. Deal, T. Itoh and M.C. Wu, "Distributed Balanced Photodetectors for RF Photonoc Links" *International Topical Meeting on Microwave Photonics (MWP 98)*, Princeton, New Jersey, 12–14 Oct, 1998.
3. L.Y. Lin, M.C. Wu, T. Itoh, T.A. Vang, R.E. Muller, D.L. Sivco, and A.Y. Cho, "Velocity-matched distributed photodetectors with high-saturation power and large bandwidth," *IEEE Photon Technol. Lett.*, vol. **8**, no. 10, pp. 1376–1378, 1996.

CWL

4:30 pm–6:15 pm
Rooms 314/315

Ultrafast Material Dynamics

Arthur L. Smirl, *University of Iowa, USA, Presider*

CWL1 4:30 pm

Recovery dynamics of a PbS quantum dot doped glass passive mode locker

K. Wundke, J.M. Auxier, A. Schülzgen, N. Peyghambarian, N.F. Borrelli,* *Optical Sciences Center, University of Arizona, Tucson, Arizona 85721 USA; E-mail: wundke@u.arizona.edu*

Recently we demonstrated that PbS quantum dot doped glasses, fabricated by thermal treatment of an oxide molten glass,[1] can be used as intracavity saturable absorbers to obtain self-starting mode locking in infrared solid-state lasers. In particular, using these absorbers in a Cr:forsterite laser we obtained pulses as short as 4.6 *ps* with a time-bandwidth product of 0.35 and pulse energies up to 1 *nJ*.[2] Because of the large exciton Bohr radius (18 *nm*) and the small band gap energy (0.4 *meV* at RT) these saturable absorbers are suitable for operation over a wide spectral range from visible to 3 μm. However, it was unclear why shorter pulses then 4.6 *ps* could not be obtained.

Here we perform degenerate pump-probe experiments to address this point and determine the recovery time of the optical nonlinearity. The quantum dot doped glass was pumped with 120 *fs* pulses from an amplified Ti:sapphire laser system. Corresponding to the estimated intracavity power of the Cr:forsterite laser, the fluence of the pump pulse was varied from 0.1 up to 40 mJ/cm^2. The pulse wavelength was set near to the operating wavelength of the Cr:forsterite laser, i.e. near to the lowest electron-hole pair transition of the quantum dots [see Fig. 1(a)].

Fig. 1(b) shows the dynamics of the nonlinear absorption for two different pump fluences. In the pump regime above the observed mode locking threshold of the Cr:forsterite laser ($P_t \approx 0.1\ mJ/cm^2$) a two-component decay of the bleaching is observed. With increasing fluence, both decay constants τ_f and τ_s decrease. However, the relation $\tau_f \tau_s > \tau_{pulse}$ still applies for pump fluences up to forty times the threshold P_t. Recently, Kärtner et al. showed that also a slow saturable absorber can generate

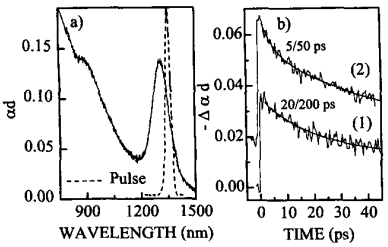

CWL1 **Fig. 1.** (a) Absorbance of the quantum dot doped glass ($d = 2\ mm$) (solid line) and spectrum of the pulses used in the pump-probe experiment (dotted line). The quantum dot size was estimated to $r \approx 5 \pm 0.05\ nm$.[3] (b) Bleaching dynamics for pump fluences of (1) 0.5 mJ/cm^2 and (2) 4 mJ/cm^2, respectively.

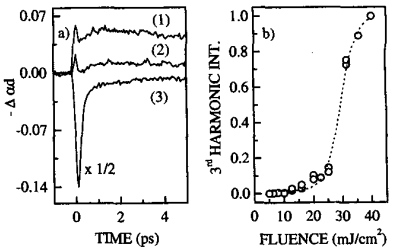

CWL1 **Fig. 2.** (a) Nonlinear absorption dynamics for pump fluences of (1) 4 mJ/cm^2, (2) 20 mJ/cm^2 and (3) 40 mJ/cm^2, respectively. (b) Normalized efficiency of the third harmonic generation in the glass host.

nearly transform-limited pulses much shorter than the absorber recovery time.[4] This theoretical result coincides with our experimental result and we can conclude that the PbS quantum dot doped glass acts as slow saturable absorber. In this case the modulation depth of the absorber mainly limits the pulse width.

The shortening of τ_f with increasing fluence down to the time scale of the laser pulse width suggests a possible transition from a slow to a fast saturable absorber. Unfortunately, in our experiments, above a certain pump power the mode locking becomes unstable, even though we did not observe oversaturation of the absorber.

To explain this behavior we show in Fig. 2(a) the nonlinear absorption for highest pump fluences. A clear departure from the simple bleaching effect is observed which completely dominates the nonlinearity at highest intensities. This effect coincides with the observation of bright 3^{rd}-harmonic generation in the glass host [see Fig. 2(b)], and limits the modulation depth of the saturable absorber to about 50%, thus limiting the pulse width. Based on this result we believe that the performance of the saturable absorber can be improved either by increasing the quantum dot concentration or by reducing the concentration of the heavy metal Pb in the glass and therefore reducing the large $\chi^{(3)}$.[5]

We acknowledge support from COEDIP and Corning Inc..

*Technology Group, Corning Inc., Research and Development Center, Sullivan Park, Corning, New York 14831, USA